ACS OMEGA

Article

Cite This: ACS Omega 2018, 3, 744−752

Tailoring Nanofluid Thermophysical Profile through Graphene Nanoplatelets Surface Functionalization

Carolina Hermida-Merino,[†] Martín Pérez-Rodríguez,[†] Ana B. Pereiro,[‡] Manuel M. Piñeiro,*[,†] and María José Pastoriza-Gallego*[,†]

[†]Departamento de Física Aplicada, Universidade de Vigo, Campus Lagoas-Marcosende, E36310 Vigo, Spain

[‡]Alternative Fluids for Green Chemistry Unit, LAQV, REQUIMTE, Department of Chemistry, Faculdade de Ciências e Tecnologia, FCT/UNL, Universidade Nova de Lisboa, Campus da Caparica, 2829-516 Caparica, Portugal

ABSTRACT: In this study, the effect of chemical surface functionalization through oxidation of exfoliated graphite nanoplatelets in the transport properties of their aqueous nanofluids has been analyzed. With this objective, thermal conductivity and viscoelastic properties have been determined for original and oxidized nanoplatelets. The results show that the functionalization completely changes the internal structure of the suspension, which is reflected in shifts of even orders of magnitude on viscosity, yield stress, or storage or loss moduli. It is evident that this influences thermal conduction properties as well, as it has been also demonstrated. This shows that nanostructure surface functionalization can be a useful strategy to tune nanofluid thermophysical properties.

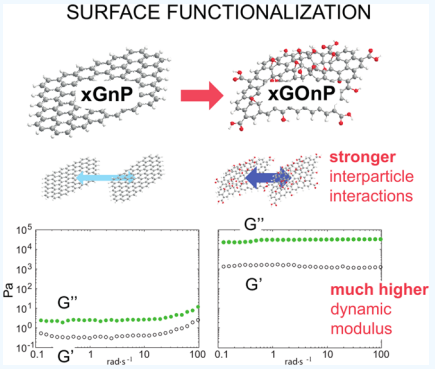

INTRODUCTION

The use of graphene nanoplatelets to produce nanofluids (NFs hereafter), nanometric-scale particle colloidal dispersions, has been recently proposed, and the studies published so far suggest that their performance as technical fluids in different industrial applications is promising. Although a relatively emerging topic, the number of concerned papers published is remarkable, and some reviews have been already published, as for instance, those by Rasheed et al.[1] or Sadeghinezhad et al.[2] The addition of graphene nanoplatelets to a base fluid has been proposed to improve lubrication conditions[3,4] or to enhance the heat-transfer properties of a base fluid.[5,6] This use of graphene can be regarded as a particular path within the active field of NF characterization, where the use of nanostructures of very different nature has been tested, and this includes a variety of carbon allotropes, such as nanotubes,[7] either single-[8] or multiwalled,[9] graphite,[10] graphene,[11] or graphene oxide.[12]

Despite the considerable number of studies related with NFs (some recent reviews as those of Murshed and de Castro[13] or Eggers and Kabelac[14] are representative of the current status of the field), many critical questions are a matter of open debate. The original motivations for these studies were the supposed enhanced heat-conducting properties of these suspensions, with unexpectedly huge reported experimental heat conductivities that exceeded sometimes by more than 1 order of magnitude of the expected values. Despite the fact that it was later demonstrated that this enhancement was not as fabulous as declared, this initial impulse attracted attention of other NF properties, as for instance, viscosity, rheological behavior, heat capacity, etc., which also exhibit unexpected and nonclassical trends. The broadening of the scope of research has brought interesting insights that are unveiling amazing physics leading to many practical applications.[15] It is worth saying that nowadays the interest on NF research goes much further than the determination of their still intriguing heat-transfer properties.

Concerning the use of graphene in this context, its presentation[16] is the first issue and undoubtedly a crucial one. Obtaining dispersed single-layer nanosheets is difficult to achieve due to aggregation, and often the suspended material consists actually of exfoliated graphite nanoparticles (xGnPs),[17,18] whose use is very convenient for its price and ease of preparation and handling. As with other nanoparticles, the stability of the suspensions obtained is generally poor. If water is used as base fluid, the stability of xGnP is reduced, and it is improved when other fluids, such as ethylene glycol,[19,20] are used as dispersing medium. The use of xGnP produces interesting effects on the base fluid viscosity trends, and it has been shown[19] that non-Newtonian behavior appears even at low charge loads, showing shear thinning and dynamic yield stress. This is the result of a remarkable structure within the colloid. An estimation of the fractal dimension of the aggregates in that case results in the conclusion that a reaction-limited chain aggregation (RLCA)-type aggregation process occurs. This imposes serious limitations to the practical use of these working fluids in any application, including fluid flow, as viscosity may vary over a range of several orders of magnitude,

Received: October 31, 2017
Accepted: January 4, 2018
Published: January 22, 2018

DOI: 10.1021/acsomega.7b01681
ACS Omega 2018, 3, 744−752

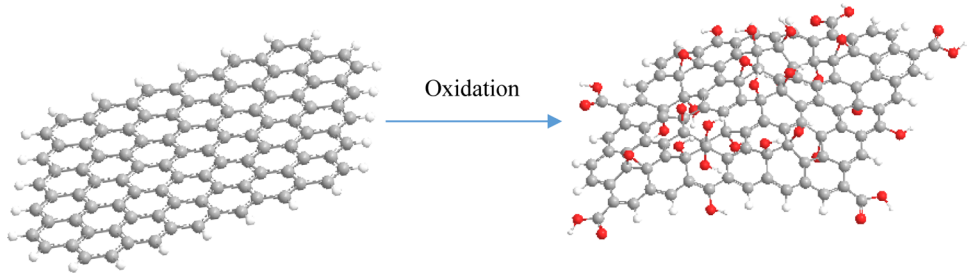

Figure 1. Scheme of a small graphene monolayer showing the main feature in xGOnP: structure flexibility, loss of aromaticity in substitution sites, and the presence of oxygen (red circles) containing functional groups, such as epoxy, hydroxyl, and carboxyl.

reaching a surprising "solidlike" plastic behavior that may completely hinder flow.

A feasible option to control xGnP NF stability and aggregation is the tuning of interface properties between the carbon and the base fluid, and this can be achieved by the chemical modification of the carbon surface by either the chemical functionalization of the surface or the induction of chemical bonding. In particular, oxidation reactions have been used frequently, obtained by different techniques.[21−24] In a previous work,[25] a mild oxidation pathway was used to obtain oxidized xGnP (named xGOnP). Nitric acid was then used, varying the process conditions, which strongly reacts with the aromatic carbon structures, producing oxygenated functional groups, such as carboxyl and ketones.[26] The resulting nanoparticles were analyzed by thermogravimetric analysis (TGA), X-ray spectroscopy, and Raman spectroscopy, and the morphology was studied by electron microscopy. The stability in water in this case was much better than that for the original xGnP, and this NF electrical conductivity was determined, finding that the conditions of the surface functionalization could be used as a route to tune this property, enabling a controlled tailoring of the suspension conditions.

Now, an analysis of the influence of surface treatment on the thermal conductivity and rheological properties of the NF obtained using again water as base fluid is the objective. The so-called transient hot-wire method is one of the most widely used techniques for determining fluid thermal conductivity.[27,28] In the case of nanofluids, ease of use and the relative accuracy of this technique have made it very popular, and most of the published scientific papers on the characterization of nanofluid thermal conductivity use this experimental technique.[29−31] The shear viscosity of the NFs obtained from the original Newtonian base fluids may have a Newton shell and a shear shell, depending on a number of factors. Some of them are the material, size, shape, and concentration of nanoparticles as well as the type of liquid base. Structured fluids such as colloidal gels, microgel suspensions, dense suspensions, concentrated emulsions, and foams are viscoplastic deformation fluids, and the trend of the viscoelastic properties provides useful information to determine the nature of the interactions. In this case, it will be discussed if the surface functionalization of the xGnP can be used to design new working fluids with a thermophysical profile adapted to the particular needs of a given application.

RESULTS AND DISCUSSION

Characterization. The complete characterization of the xGOnP using electron microscopy, thermogravimetric analysis (TGA), and X-ray photoelectron spectroscopy has been presented in an earlier publication.[25] Summarizing this characterization, Figure 1 presents a sketch of the morphological model for the oxidized nanoplatelets. A small section of a platelet is presented, small enough to show the main characteristics, which can be extended in the plane and combined in several layers to compose a randomly chosen real xGOnP. As a result of the oxidation process, epoxy, hydroxyl, and carboxyl groups are attached to the NP surface. The surface density of these groups can be determined by changing the oxydation process conditions and adequately quantified by the described characterization techniques. This process produces as first results an improvement of the stability in polar base fluids, such as water. In addition, in a previous work,[25] it was shown that the effect of this surface functionalization on the electrical conductivity of aqueous suspensions was very remarkable. It was observed that xGOnP produces an increase in the NF electric conductivity, as the oxidized moieties dissociate showing a weak acid behavior. This implies that the oxidation process can be used to control the NF electrical conductivity. The effect of this oxidation process on other thermophysical properties has not been studied in detail yet, but it can be used as a method to tailor NF thermophysical properties.

The stability of xGnP/H_2O and xGOnP/H_2O NFs was evaluated using a Helios Omega UV−vis spectrophotometer equipped with a thermostated cell carrier at different sonication times for further determination of the ζ potential, as described in a previous work.[25] The stability of xGnP/H_2O samples is clearly worse, needing higher sonication times, but in any case, it is enough in all cases to ensure sample stability during the performed experimental runs.

Thermal Conductivity. The results obtained for xGOnP and xGnP NFs show that the thermal conductivity increases with concentration. The improvement in thermal conductivity (κ_{nf}/κ_0) vs concentration is shown in Figure 2. Table 1 shows the weight and volume fractions of xGnP and xGOnP for all concentrations at a temperature of 293.15 K, showing the thermal conductivity measured for each case. In this case, the improvement in the thermal conductivity of the xGOnP samples must be underlined, as the difference of the slope with volume concentration is very remarkable compared to the original xGnP NF. The use of surfactants or stabilizers is very common to improve the stability of NFs. This is important for the evaluation of their performance in practical applications, but the use of these additives produces a shift in the NF thermophysical properties, and so, for characterization purposes, the use of surfactants adds an extra variable to be kept in mind. For example, Selvam et al.[32] measured the thermal conductivity of water- and ethylene glycol-based xGnP NFs obtained using sodium deoxycholate as dispersing agent. A comparison of their experimental data reveals that the thermal

DOI: 10.1021/acsomega.7b01681
ACS Omega 2018, 3, 744−752

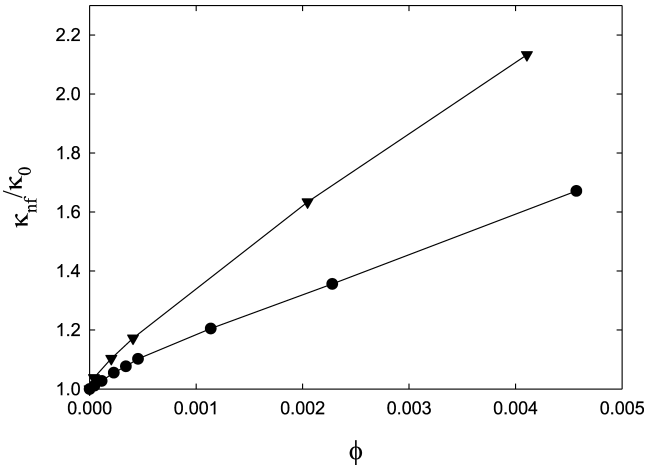

Figure 2. Thermal conductivity enhancement (κ_{nf}/κ_0) vs NF volume fraction at 293.15 K: ●, xGnP; ▼, xGOnP.

Table 1. Thermal Conductivity (κ, W·m^{-1}·K^{-1}) Values Measured at 293.15 K for the xGnP and xGOnP Nanofluids

volume fraction (ϕ)	% wt	κ
	xGnP	
0.000000	0.000	0.59920
0.000046	0.010	0.60600
0.000114	0.025	0.61570
0.000227	0.050	0.63230
0.000341	0.075	0.64533
0.000455	0.100	0.66050
0.001138	0.250	0.72200
0.002279	0.500	0.81250
0.004570	1.000	1.00150
	xGOnP	
0.000000	0.000	0.59920
0.000041	0.010	0.62200
0.000204	0.050	0.66100
0.000408	0.100	0.70250
0.002050	0.500	0.97900
0.004110	1.000	1.27800

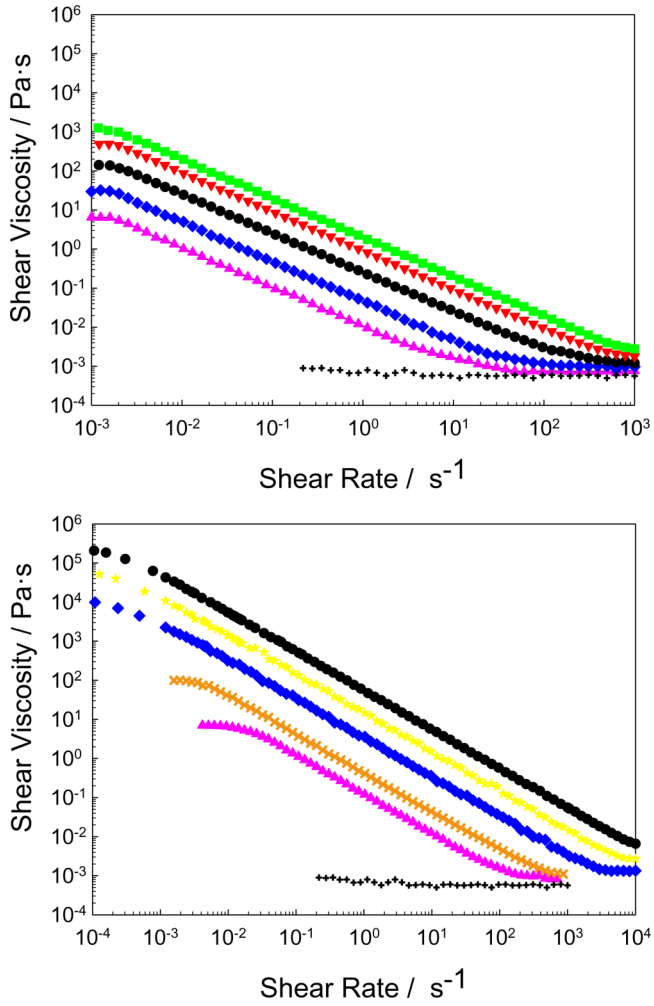

Figure 3. Shear viscosity (η) vs shear rate ($\dot{\gamma}$) of xGnP/H_2O (A) and xGOnP/H_2O (B) NFs at 293.15 K for different weight fractions: +, water; ▲, 0.1 wt %; ×, 0.25 wt %; ♦, 0.5 wt %; ★, 0.75 wt %; ●, 1 wt %; ▼, 2 wt %; and ■, 3 wt %.

conductivity of their water NFs is slightly lower than that of the samples studied in this work, and the difference can be attributed in this case to the use of the surfactant.

The comparison of thermal conductivity values of other aqueous graphene NFs is not straightforward as many variables are involved in the sample preparation. Nevertheless, the presented data agree well with other recent references, and for instance, Ahammed et al.[33] reported a 16.04% enhancement in κ value for xGnP/H_2O NF at 0.1% in volume fraction, whereas our experimental value corresponds to a 18.42% enhancement. For the case of xGOnP/H_2O NF, Hajjar et al.[34] reported a 15.25% enhancement in κ at 0.1% weight concentration, whereas our experimental value corresponds to a 17.23% enhancement.

Nonlinear Viscoelastic Measurements. Figure 3 shows shear viscosity (η) as a function of shear rate ($\dot{\gamma}$), usually referred to as flow curves, of H_2O and three different weight fractions of xGnP/H_2O and xGOnP/H_2O NFs (1, 2, 3 and 0.1, 0.5, 1 wt %, respectively). H_2O is a Newtonian fluid, but both NFs show shear thinning with yield stress even at very low concentrations, which represents a non-Newtonian behavior, as shear viscosity decreases with the applied shear rate. As concentration increases, a Newtonian plateau appears in the lowest $\dot{\gamma}$ region, and the shear thinning is more pronounced due to the stronger sheet−sheet and multisheet interactions with the increase in concentration. Shear thinning of well-dispersed suspensions is related with modifications in the structure and arrangement of interacting particles. Shearing may cause the particles to orient in the direction of flow and its gradient, breaking agglomerates and reducing the amount of immobilized solvent. Interaction forces then decrease, thereby decreasing also the flow resistance and the apparent viscosity of the system. A comparison of the viscosity trends shows that the oxidation process produces an increase in viscosity, especially in the low-shear region, of up to 3 orders of magnitude.

Certain non-Newtonian materials exhibit the so-called yield stress, absorbing when shearing starts stress energy without flowing, until the yield stress threshold is exceeded and then deformation occurs. This observed behavior can be associated with the reorientation of exfoliated graphite nanosheets at high shear rates. According to this short-range order, these materials behave as solids when the local shear is below the yield stress, but once it is exceeded, flow occurs with a nonlinear stress−strain relationship.

DOI: 10.1021/acsomega.7b01681
ACS Omega 2018, 3, 744−752

The yield stress value for a certain fluid can be obtained as an extrapolation of the shear stress value at zero shear rate, but the ideal rheological models with yield stress present two limitations. First, there is a singularity for viscosity when the strain is zero, and, in some cases, the viscosity function is not activated in the limit of zero strain rate. Papanastasiou[35] proposed a model to overcome the limitation due to the uniqueness of the viscosity for $\gamma \rightarrow 0$ by proposing an exponential regularization for the term of the creep stress of the Bingham model.[36] The same idea has subsequently been used with the Herschel–Bulkley model.[37] This model describes in a single equation the creep and noncreep zones and allows the determination of yield stress σ_y

$$\sigma = \sigma_y[1 - e^{-m\dot{\gamma}}] + K\dot{\gamma}^p \quad (1)$$

Figure 4 shows the experimental shear stress vs shear rate of xGnP/H_2O and xGOnP/H_2O NFs at different concentrations (0.1, 0.5, 1, 2, and 3% by weight for xGnP and 0.1, 0.25, 0.5, 0.75, and 1% for xGOnP) and their fit with the Papanastasiou model. The dynamic yield stress values obtained from this fit are shown in Table 2. These values increase nearly exponentially with weight fraction. At the same weight fraction (1 wt %), xGOnP NFs show a dynamic yield stress 2 orders of magnitude higher, evidencing an internal structure that is completely different (and stronger) from the case of original xGnP NFs.

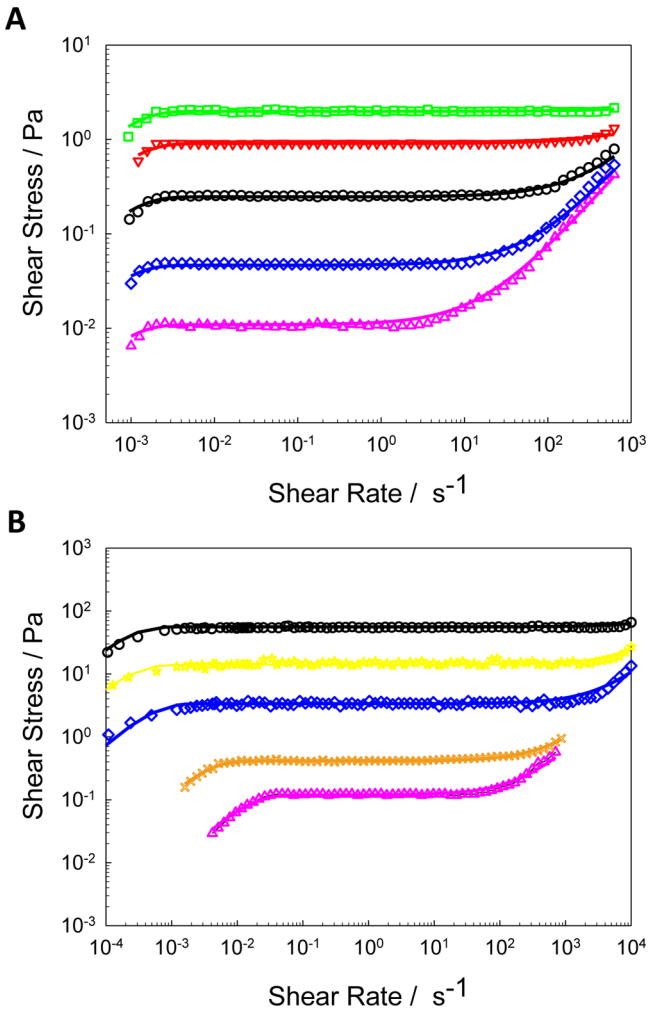

Figure 4. Shear stress vs shear rate $\dot{\gamma}$ of xGnP/H_2O (A) and xGOnP/H_2O (B) NFs at 293.15 K for different weight fractions: △, 0.1 wt %; ×, 0.25 wt %; ◊, 0.5 wt %; ☆, 0.75 wt %; ○, 1 wt %; ▽, 2 wt %; and □, 3 wt %. The solid lines represent the fit using Papanastasiou's modification of the Herschel–Bulkley model.

Table 2. Yield Stress σ_y Values Determined for xGnP/H_2O and xGOnP/H_2O NFs at 293.15 K and Different Weight Fractions

weight fraction (wt %)	yield stress (σ_y, Pa)
xGnP	
0.10	0.011 ± 0.005
0.50	0.047 ± 0.006
1.00	0.247 ± 0.008
2.00	0.905 ± 0.009
3.00	1.990 ± 0.020
xGOnP	
0.10	0.119 ± 0.008
0.25	0.415 ± 0.009
0.50	3.370 ± 0.030
0.75	14.000 ± 0.200
1.00	56.000 ± 0.400

Linear Viscoelastic Measurements. *Strain Sweep Tests.* Oscillatory or dynamic experiments were then performed to determine the viscoelastic behavior. This way, stress can be separated into its elastic and viscous contributions, obtaining the elastic or storage modulus, G', and the viscous or loss modulus, G'', plotted in Figure 5. First, strain sweep tests at constant ω = 10 rad·s^{-1} were carried out to identify the linear viscoelastic region (LVR) in the strain range of 0.1–1000%. The linear regime, where G' and G'' are independent of strain amplitude, is then determined. G' decreases monotonically as strain increases, whereas G'' goes through a maximum. This means that when an external strain is imposed, the structure of both NFs resists the deformation up to the critical strain value, where G'' increases; then, the structure is lost by the disaggregation of nanoparticles and the sample flows, decreasing both G' and G''. The moduli of both G' and G'' at the same weight fraction for xGOnP are 4 orders of magnitude larger than those for xGnP, again evidencing a much stronger structure. This remarkable difference can be attributed to the existence of a more complex structure of aggregates network in the xGOnP nanofluids, as will be discussed later.

Stress–strain curves can also be plotted, as it has been done for xGOnP NFs in Figure 6. The deviation from linearity in this plot allows the determination of static yield stress and critical strain values listed in Table 3. Static yield stress values increase linearly (in logarithmic scale) with volume fraction, and critical strain values decrease linearly with volume fraction.

Analysis of the Fractal Dimension. An analysis of the dependence of G' on the volume fraction is useful to discuss the fluid internal structure. Colloidal gels are formed by particle aggregation and show viscoelasticity; their behavior with the volume fraction is governed by the fractal nature of the colloidal flocks. The gel network is considered to be a collection of fractal flocks closely packed throughout the sample. Shih et al.[38] developed a scaling model relating G' and the critical strain to the particle volume fraction for a colloidal gel far from the gelation threshold.

The fractal dimension, or Hausdorff dimension, is a generalization of the dimension of a real vector space (Euclidean or topological dimension) based on the local

DOI: 10.1021/acsomega.7b01681
ACS Omega 2018, 3, 744–752

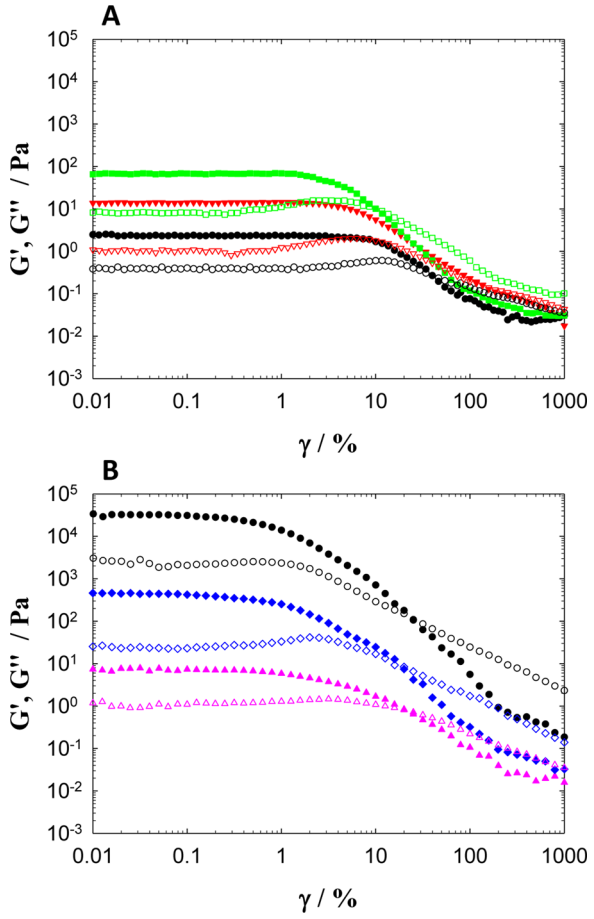

Figure 5. Storage (G', filled symbols) and loss (G'', empty symbols) moduli vs strain (γ) at 10 rad·s^{-1} and 293.15 K of xGnP/H_2O (A) and xGOnP/H_2O (B) NFs for different weight fractions: △, 0.1 wt %; ◊, 0.5 wt %; ○, 1 wt %; ▽, 2 wt %; and □, 3 wt %.

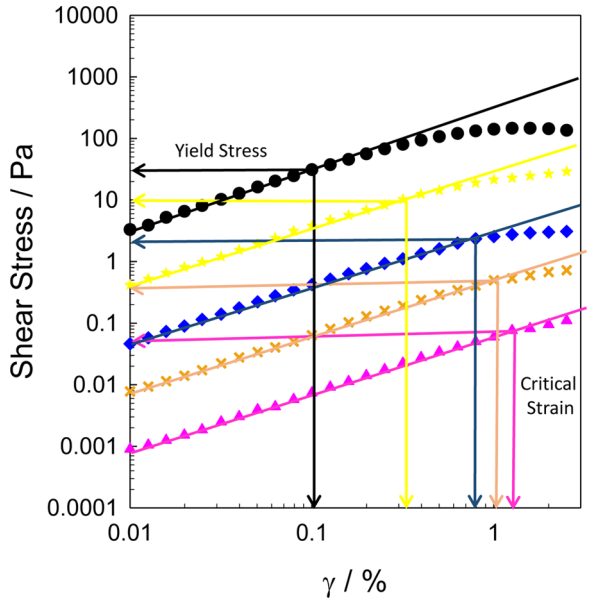

Figure 6. Shear stress vs strain (γ) at 10 rad·s^{-1} and 293.15 K of xGOnP/H_2O NFs for different weight fractions: ●, 1 wt %; ★, 0.75 wt %; ♦, 0.5 wt %; ×, 0.25 wt %; and ▲, 0.1 wt %.

measurement of a set. Fractal sets of points typically show noninteger Hausdorff dimensions because of the scale

Table 3. Static Yield Stress (Y) and Critical Strain (γ_c) Values for Different xGOnP/H_2O and xGnP/H_2O NFs at 293.15 K and ω = 10 rad·s^{-1}

weight fraction (wt %)	volume fraction (ϕ, v/v)	static yield stress (Y, Pa)	critical strain (γ_c, %)
	xGOnP		
0.10	0.0004084	0.0761	1.260
0.25	0.0010219	0.4980	1.000
0.50	0.0020469	2.3500	0.734
0.75	0.0030749	12.5000	0.398
1.00	0.0041059	31.0000	0.100
	xGnP		
0.50	0.0165	0.021	3.16
1.00	0.0326	0.068	2.82
1.50	0.0483	0.142	2.47
2.00	0.0637	0.315	2.10
2.50	0.0787	0.563	1.73
3.00	0.0935	0.930	1.36

invariance of their geometric structure, extending the concept of line, plane, and volume to objects of arbitrary dimension between them. The analysis of fractal dimension of the aggregates helps to obtain valuable information about their structure: first of all, it provides a picture of some aspects of the geometry, if it is ordered in linear chains, planes, or three-dimensional flocks, and their relative density, but at the same time allows identifying the aggregation mechanism. Then, according to Shih et al.,[38] the fractal dimension of the aggregates can be calculated using the relation between yield stress (Y) and the nanoparticles volume fraction (ϕ) in the suspension

$$Y = \alpha\phi^m \tag{2}$$

where α is a coefficient depending on ζ potential and the interparticle average distance and m is related to the fractal dimension of the flocculated network (D_f) as

$$m = (d + X)/(d - D_f) \tag{3}$$

where X and d are, respectively, the aggregate backbone dimension of the whole system and the Euclidean dimension of the system (in this case, d = 3). The dimension values obtained allowed to analyze the type of aggregation and structure properties. The relations between molar volume and yield stress are represented in Figure 7 for both xGnP and xGOnP NFs. These experimental data were fitted to eq 2, obtaining m = 2.80 ± 0.08 for xGnP and m = 3.25 ± 0.14 for xGOnP. These values yield fractal dimensions $D_f^{(xGnP)}$ = 1.23 and $D_f^{(xGOnP)}$ = 1.46 when we consider the backbone dimension to be X = 2.

The fractal dimension found previously[19] for xGnP/EG considering X = 2 was 2.36, one unity larger than the value considering H_2O as base fluid. To explain this discrepancy, it is convenient to take into consideration the values of D_f for all possible backbone dimensions. Consequently, supplementary calculations were done, obtaining $D_f^{(xGnP)}$ (1) = 1.57, $D_f^{(xGOnP)}$ (1) = 1.77 for X = 1, $D_f^{(xGnP)}$ (3) = 0.86, and $D_f^{(xGOnP)}$ (3) = 1.15 for X = 3. All of them are represented in Figure 8 and compared to reference values. Although three-dimensional backbone is hardly assumable, the corresponding values were also included for completeness.

The calculated values of D_f considering X = 1 or 2 lay between 1 and 2, corresponding to a structure between a line and a plane. For X = 1, these values are close to 1.8 (especially

DOI: 10.1021/acsomega.7b01681
ACS Omega 2018, 3, 744−752

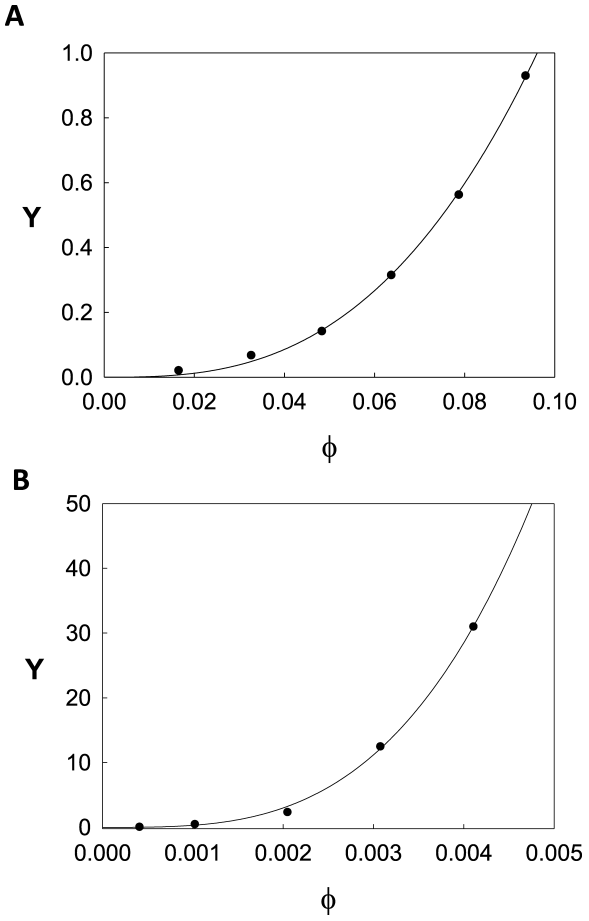

Figure 7. Static yield stress (Y) as a function of volume fraction ϕ for both xGnP (A) and xGOnP (B) NFs. Experimental data (●) were fitted to eq 2, obtaining the solid lines.

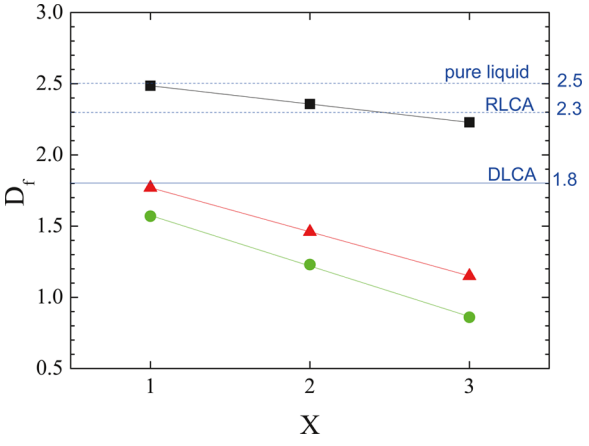

Figure 8. Fractal dimension of aggregates (D_f) as a function of supposed backbone dimension (X). ■ correspond to xGnP/EG,[19] ● to xGnP/H_2O, and ▲ to xGOnP/H_2O. D_f characteristic values of pure liquid, RLCA, and diffusion-limited cluster aggregation (DLCA) are included for reference.

for the case of xGOnP), which is the characteristic dimension of diffusion-limited cluster aggregation (DLCA). This result is clearly opposed to the results obtained for xGnP/EG,[19] which were much closer to 2.3, corresponding in that case to a reaction-limited cluster aggregation (RLCA) process. Results independent of the backbone dimension considered strongly suggest that the aggregation present is of the RLCA type, building compact structures with effective dimension greater than 2. Moreover, the high value obtained for n is also characteristic of this aggregation scheme.

The large difference observed in the fractal dimensions of xGnP between the present study and the previous one may be explained directly by the relation between particle−particle and particle−solvent forces, due to the organic behavior of EG in contrast with the polar character of H_2O. In the case of xGnP/EG, the fractal dimension was found to be between a plane and a solid. Solvent tends to dilute the aggregates because of their hydrophobic surface as well as the solvent character, and as a consequence, the resulting structure will be sparse and complex. Due to the lack of resistance of the solvent to the extension of the planar particles, their conformation is mainly entropy-driven, allowing for a two-dimensional network backbone. H_2O, on the other hand, tends to repel graphene nanoparticles due its characteristic polar nature. More spherical and closed structures are expected to form driven by H_2O repulsion, behaving much more like micelles than small sheets. The aggregates network will present a dynamic behavior resembling DLCA, typical of chainlike or dendritic aggregates of spherical beads. The relation between intermolecular forces explains also the larger values of fractal dimension in oxidized nanoparticles. The increase in the number of polar moieties in the surface of xGOnP with respect to xGnP decreases their average hydrophobic character, enhancing solubility in water and allowing for a more complex and developed structure of aggregates network.

Frequency Sweep Tests. Finally, frequency sweep tests were carried out in the LVR, with angular frequencies ranging from 0.1 to 400 rad·s^{-1} and a constant strain value of 0.1%. The experimental data of storage and loss moduli are shown in Figure 9. For these NFs, the storage modulus exceeds the loss modulus, $G' > G''$, especially for higher concentrations, and G' values are practically constant in the whole frequency range in both cases, indicating a typical gel structure and the dominant elastic nature of the material under these conditions. For the case of xGnP, both moduli increase with concentration at a given constant frequency. In addition, they increase slightly with frequency beyond an approximate value of 10 rad·s^{-1}. These results must be underlined because the addition of nanoparticles produces, even at low concentrations and frequencies, a continuous transition toward elastic behavior. On the other hand, for the case of xGOnP, both moduli are constant within the frequency range studied, showing a clear solidlike behavior. Both G' and G'' are now, if compared to the previous case, and for the same concentration, 4 orders of magnitude higher, which underlines the dramatic behavior change produced by the nanosheets oxidation. This means that rheological studies of its viscoelastic nature are essential to determine its potential practical use for any technical application.

The experimental data for G' at low frequencies can be modeled as a function of concentration according to a percolation expression as follows[39]

$$\log(G') = A + B\log(\phi - \phi_0) \quad (4)$$

where A and B are constants and ϕ_0 is the threshold volume fraction, and the equation can be applied only near the percolation threshold.

Experimental data measured at low frequency (10 rad·s^{-1}) were fitted to eq 4, leaving as adjustable parameters the

DOI: 10.1021/acsomega.7b01681
ACS Omega 2018, 3, 744−752

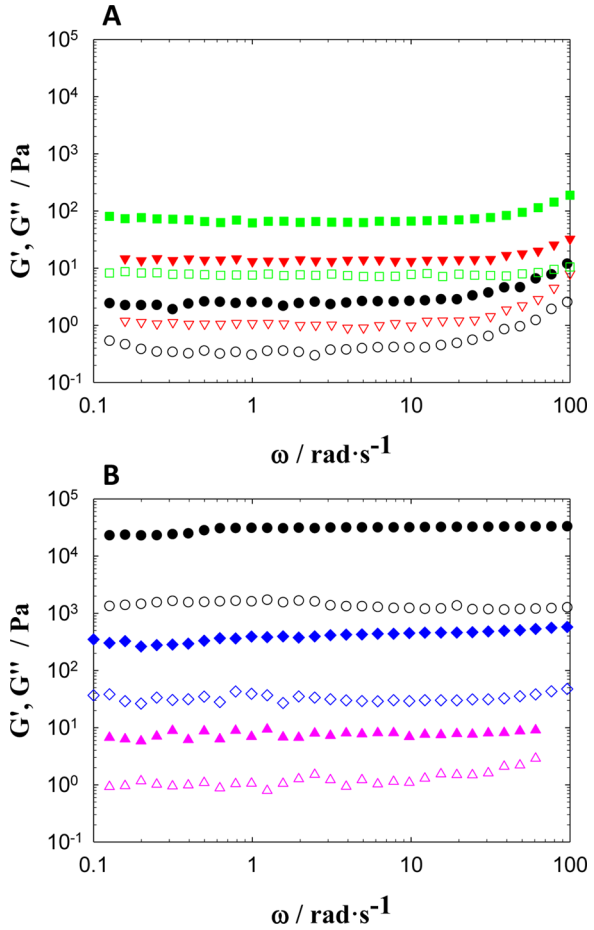

Figure 9. Storage (G', filled symbols) and loss (G'', empty symbols) moduli vs angular frequency (ω) at a constant strain (0.1%) and 293.15 K of xGnP/H_2O (A) and xGOnP/H_2O (B) NFs for different weight fractions: △, 0.1 wt %; ◊, 0.5 wt %; ○, 1 wt %; ▽, 2 wt %; □, 3 wt %.

concentration at the threshold (ϕ_0) and the parameters A and B. For NFs, a linear relation has been obtained between the logarithm of the storage modulus G' and the volume fraction. As shown in Figure 10, the experimental data are adequately represented by eq 4, from which a close-to-zero critical concentration is determined for both cases. Therefore, these experiments have been performed at concentrations that are well beyond the percolation threshold and can be easily classified as gels. For these exfoliated graphite NFs, the van der Waals interactions are so strong that induce large structures even at very low concentrations.

CONCLUSIONS

The important effect of oxidation on exfoliated graphite platelets NF thermal conductivity has to be emphasized because the trend against volume fraction concentration changes remarkably when comparing with the original xGnP/H_2O NF. Higher conductivity values are obtained with lower nanoparticle loads, an important feature for their practical applications. The difference in dry sintered nanosheet density produces that the same weight fraction produces an effective lower volume fraction for the case of xGOnP NF, showing a remarkable thermal conductivity enhancement compared to the equivalent volume fraction for the xGnP case.

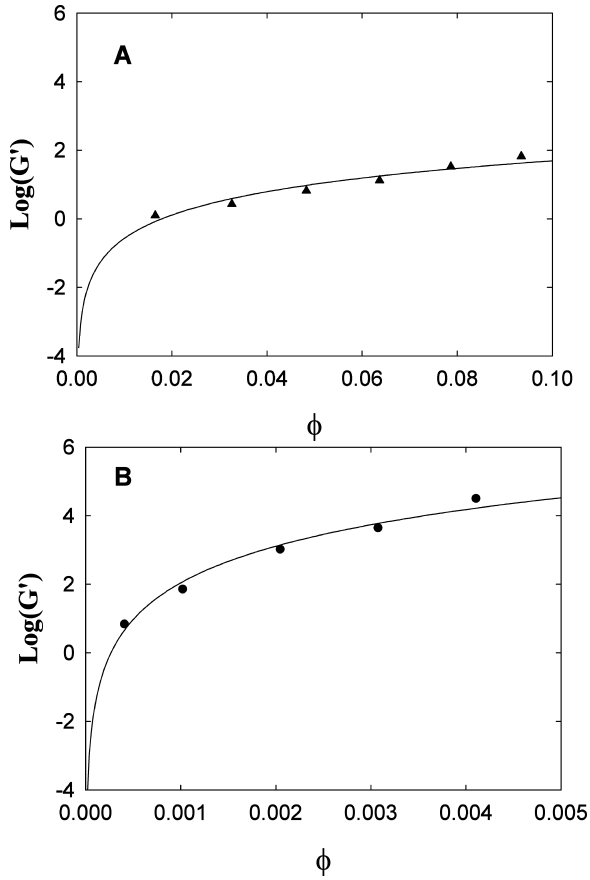

Figure 10. Logarithmic storage modulus, log(G'), vs volume fraction of xGnP/H_2O (A) and xGOnP/H_2O (B) NFs fitted using the percolation model (eq 4) at 10 rad·s^{-1} and 293.15 K with 0.1% of strain.

The non-Newtonian nature of xGnP/H_2O and xGOnP/H_2O NFs is evident, showing shear thinning and dynamic yield stress. All samples show viscoplastic nature suggesting that a combination of particle aggregation and shape effects is the mechanism for its high-shear rheological behavior, which is also supported by the thermal conductivity measurements. G' decreases after a certain critical strain, and G'' presents an overshoot phenomenon.

Strain sweep tests show that structural interactions within xGOnP NFs are remarkably much stronger than in the case of nonoxidized nanoplatelets, yielding loss and elastic moduli 4 orders of magnitude higher. This change in the internal structure of the NF caused by the surface functionalization process has to be highlighted.

As a continuation of these tests, the aggregates fractal dimension D_f has been calculated, obtaining a value very close to the characteristic DLCA theory value, especially for the xGOnP case. This value is characteristic of chainlike or dendritic aggregates. The increase of surface-adsorbed oxygen-containing functional groups for the case of xGOnP decreases nanosheet hydrophobicity, enhancing solubility and thus allowing a more complex and developed aggregates structure. Frequency sweep tests confirm the cited stronger internal structure in the case of xGOnP NFs. In addition, the close-to-zero critical concentration values determined for both cases evidence that even for xGnP interparticle interactions are so intense that produce a well-defined structure even at very low concentrations.

DOI: 10.1021/acsomega.7b01681
ACS Omega 2018, 3, 744−752

The objective of this work is the evaluation of graphene surface functionalization through oxidation as a tool to tailor the derived NF thermal profile as industrial working fluid. The final conclusion is that the effects of this functionalization can be regarded as somewhat contradictory. Although thermal conductivity is clearly enhanced and can be tuned by adjusting the surface chemical treatment, the viscoelastic behavior of the samples changes, producing higher viscosity due to the evident changes in the NF internal structure. These changes are induced by the different aggregation processes occurring in the case of xGnP and xGOnP nanoplatelets. The competition of these two factors has to be carefully taken into account for practical purposes as tailoring an NF to increase thermal conductivity without evaluating other properties, as the rheological profile may induce an incomplete evaluation of the working fluid potential performance.

EXPERIMENTAL SECTION

Chemicals and Materials. Exfoliated graphite nanoplatelets (xGnPs) grade C were supplied by XG Sciences, Inc. The declared surface area is approximately 750 $mm^2 \cdot g^{-1}$, and the nominal flake thickness is 1−5 nm. Nitric acid (HNO_3, analytical grade) was supplied by Aldrich (99%). Aqueous solutions were prepared with Milli-Q-grade water. Exfoliated graphite oxide nanosheets (xGOnPs) were synthesized from xGnP through reaction with nitric acid, as detailed in a previous work.[25] Using these nanoplatelets, homogeneous and stable suspensions of xGnP/H_2O and xGOnP/H_2O were prepared. The nanopowder was weighed using a Mettler AE-240 electronic balance with an accuracy of 5×10^{-5} g and then dispersed into a predetermined volume of the base fluid to obtain the desired weight fraction of up to 1 wt %, and the particles were dispersed using an ultrasonic bath (Clifton, 80 W). The stability of the suspensions prepared using different sonication times was evaluated using an Agilent HP 8453 UV−vis spectrophotometer.

The thermal conductivity of the samples has been determined by a device based on transient hot-wire technology at 293.15 K for concentrations up to 1% by weight using a Decagon-compatible KD2 thermal conductivity meter. This device is based on the transient hot-wire technology,[40] which is widely used in the field of NFs because it minimizes the problems of natural convection and the influence of the conductive final effects and presents a reduced measurement time, much lower than the characteristic sedimentation times. Further details regarding the measurement procedure can be found in previous works.[41,42] Despite the fact that this device is widely used for NF measurements, the limitations of the technique must be kept in mind. In a recent paper, Antoniadis et al.[43] have presented a comprehensive and rigorous analysis of the use of this technique for the case of biphasic systems obtained from the dispersion of nanometer-sized material in a fluid medium. The conclusions of the authors reveal some reasons that offer insight into the often surprising scattering observed in NF experimental thermal conductivity. Their conclusions lead to the presentation of a number of recommendations necessary to maximize data reliability. The use of double-wire probes is recommended to avoid boundary effects at the ends of the heating wire, and also the diameter of the wires should be lower than 30 μm. These two conditions are not fulfilled by the probe used in this case, but the other two recommendations (temperature rise values below 4 K and the use of insulated wires) have been respected. The device calibration performed for the base fluid yielded accurate results for the base fluid, and the result is that the thermal conductivity value determined for pure water is very accurate (κ^{exp} (293 K) = 0.59920 $W \cdot m^{-1} \cdot K^{-1}$), whereas the NIST Chemistry Webbook[44] recommended value is κ^{NIST} (293 K) = 0.59846 $W \cdot m^{-1} \cdot K^{-1}$. Concerning the NF thermal conductivity values in the Results and Discussion section, the obtained data are compared to other recent references.

Rheological properties were determined using a Physica MCR 101 rheometer (Anton Paar, Graz, Austria) equipped with a cone-plate geometry (CP 25-1) with a constant gap of 0.048 mm, allowing to control torques between 0.5 μN·m and 125 mN·m and normal force from 0.1 to 30 N. Different series of experiments were carried out to investigate the NF rheological behavior, following the procedure used previously for the characterization of other NFs.[19,45,46] Nonlinear viscoelastic experiments, or flow curves, were first determined, where shear viscosity variation with a shear rate of up to 10 000 s^{-1} is measured. Then, linear viscoelastic measurements followed, where the linear viscoelastic regime (LVR) was determined by measuring store (G')and loss (G'') moduli in the strain range of 0.01−1000% at a constant angular frequency of 10 $rad \cdot s^{-1}$, different weight fractions of up to 20 wt %, and 293.15 K. Frequency sweep measurements were also carried out from 0.1 to 600 $rad \cdot s^{-1}$ by applying a strain of 0.1% at different concentrations and 293.15 K.

AUTHOR INFORMATION

Corresponding Authors

*E-mail: mmpineiro@uvigo.es. Phone: +34 986813771 (M.M.P.).
*E-mail: mjpg@uvigo.es (M.J.P.-G.).

ORCID

Ana B. Pereiro: 0000-0001-7166-6764
Manuel M. Piñeiro: 0000-0002-3955-3564

Notes

The authors declare no competing financial interest.

ACKNOWLEDGMENTS

The authors acknowledge CACTI (Univ. de Vigo) for technical assistance with microscopy techniques and Ministerio de Economía y Competitividad, Spain, for financial support (Grant ref FIS2015-68910-P). Ana B. Pereiro wishes to thank FCT/MEC (Portugal) for financial support through her contract (Investigator FCT 2014, ref: IF/00190/2014).

REFERENCES

(1) Rasheed, A. K.; Khalid, M.; Rashmi, W.; Gupta, T. C. S. M.; Chan, A. Graphene based nanofluids and nanolubricants—Review of recent developments. *Renewable Sustainable Energy Rev.* **2016**, *63*, 346−362.

(2) Sadeghinezhad, E.; Mehrali, M.; Saidur, R.; Mehrali, M.; Latibari, S. T.; Akhiani, A. R.; Metselaar, H. S. C. A comprehensive review on graphene nanofluids: Recent research, development and applications. *Energy Convers. Manage.* **2016**, *111*, 466−487.

(3) Eswaraiah, V.; Sankaranarayanan, V.; Ramaprabhu, S. Graphene-based engine oil nanofluids for tribological applications. *ACS Appl. Mater. Interfaces* **2011**, *3*, 4221−4227.

(4) Sanes, J.; Avilés, M.-D.; Saurín, N.; Espinosa, T.; Carrión, F.-J.; Bermúdez, M.-D. Synergy between graphene and ionic liquid lubricant additives. *Tribol. Int.* **2017**, *116*, 371−382.

DOI: 10.1021/acsomega.7b01681
ACS Omega 2018, 3, 744−752

(5) Anin-Vincely, D.; Natarajan, E. Experimental investigation of the solar FPC performance using graphene oxide nanofluid under forced circulation. *Energy Convers. Manage.* **2016**, *117*, 1−11.
(6) Selvam, C.; Raja, R. S.; Lal, D. M.; Harish, S. Overall heat transfer coefficient improvement of an automobile radiator with graphene based suspensions. *Int. J. Heat Mass Transfer* **2017**, *115*, 580−588.
(7) Nasiri, A.; Shariaty-Niasar, M.; Rashidi, A.; Khodafarin, R. Effect of CNT structures on thermal conductivity and stability of nanofluid. *Int. J. Heat Mass Transfer* **2012**, *55*, 1529−1535.
(8) Nanda, J.; Maranville, C.; Bollin, S.; Sawall, D.; Ohtani, H.; Remillard, J.; Ginder, J. Thermal conductivity of single-wall carbon nanotube dispersions: role of interfacial effects. *J. Phys. Chem. C* **2008**, *112*, 654−658.
(9) Ding, Y.; Alias, H.; Wen, D.; Williams, R. A. Heat transfer of aqueous suspensions of carbon nanotubes (CNT nanofluids). *Int. J. Heat Mass Transfer* **2006**, *49*, 240−250.
(10) Yang, Y.; Zhang, Z. G.; Grulke, E. A.; Anderson, W. B.; Wu, G. Heat transfer properties of nanoparticle-in-fluid dispersions (nanofluids) in laminar flow. *Int. J.Heat Mass Transfer* **2005**, *48*, 1107−1116.
(11) Yu, W.; Xie, H.; Wang, X.; Wang, X. Significant thermal conductivity enhancement for nanofluids containing graphene nanosheets. *Phys. Lett. A* **2011**, *375*, 1323−1328.
(12) Lee, S. W.; Kim, K. M.; Bang, I. C. Study on flow boiling critical heat flux enhancement of graphene oxide/water nanofluid. *Int. J. Heat Mass Transfer* **2013**, *65*, 348−356.
(13) Murshed, S. M. S., de Castro, C. A. N., Eds. *Nanofluids, Synthesis, Properties and Applications*; Nova Science Publishers, Inc.: NY, 2014.
(14) Eggers, J. R.; Kabelac, S. Nanofluids revisited. *Appl. Therm. Eng.* **2016**, *106*, 1114−1126.
(15) Kostic, M. M. Critical Issues in Nanofluids Research and Application Potentials. In *Nanofluids*; Zhang, Y., Ed.; Nova Science Publishers, 2013; Chapter 1, pp 1−49.
(16) Bianco, A.; Cheng, H.-M.; Enoki, T.; Gogotsi, Y.; Hurt, R.; Koratkar, N.; Kyotani, T.; Monthioux, M.; Park, C.; Tascon, J.; et al. All in the graphene family - A recommended nomenclature for two-dimensional carbon materials. *Carbon* **2013**, *65*, 1−6.
(17) Zhu, Y.; Murali, S.; Cai, W.; Li, X.; Suk, J. W.; Potts, J. R.; Ruoff, R. S. Graphene and graphene oxide: synthesis, properties, and applications. *Adv. Mater.* **2010**, *22*, 3906−3924.
(18) Chung, D. A review of exfoliated graphite. *J. Mater. Sci.* **2016**, *51*, 554−568.
(19) Hermida-Merino, C.; Pérez-Rodríguez, M.; Piñeiro, M. M.; Pastoriza-Gallego, M. J. Evidence of viscoplastic behavior of exfoliated graphite nanofluids. *Soft Matter* **2016**, *12*, 2264−2275.
(20) Cabaleiro, D.; Colla, L.; Barison, S.; Lugo, L.; Fedele, L.; Bobbo, S. Heat Transfer Capability of (Ethylene Glycol + Water)-Based Nanofluids Containing Graphene Nanoplatelets: Design and Thermophysical Profile. *Nanoscale Res. Lett.* **2017**, *12*, 53.
(21) Yu, R.; Chen, L.; Liu, Q.; Lin, J.; Tan, K.-L.; Ng, S.; Chan, H.; Xu, G.-Q.; Hor, T. Platinum Deposition on Carbon Nanotubes via Chemical Modification. *Chem. Mater.* **1998**, *10*, 718−722.
(22) Grujicic, M.; Cao, G.; Rao, A.; Tritt, T.; Nayak, S. UV-light enhanced oxidation of carbon nanotubes. *Appl. Surf. Sci.* **2003**, *214*, 289−303.
(23) Xia, W.; Wang, Y.; Bergsträßer, R.; Kundu, S.; Muhler, M. Surface characterization of oxygen-functionalized multi-walled carbon nanotubes by high-resolution X-ray photoelectron spectroscopy and temperature - programmed desorption. *Appl. Surf. Sci.* **2007**, *254*, 247−250.
(24) Xu, T.; Yang, J.; Liu, J.; Fu, Q. Surface modification of multi-walled carbon nanotubes by O2 plasma. *Appl. Surf. Sci.* **2007**, *253*, 8945−8951.
(25) Hermida-Merino, C.; Pérez-Rodríguez, M.; Piñeiro, M. M.; Pastoriza-Gallego, M. J. Tuning the electrical conductivity of exfoliated graphite nanosheets nanofluids by surface functionalization. *Soft Matter* **2017**, *13*, 3395−3403.
(26) Okpalugo, T.; Papakonstantinou, P.; Murphy, H.; McLaughlin, J.; Brown, N. High resolution XPS characterization of chemical functionalised MWCNTs and SWCNTs. *Carbon* **2005**, *43*, 153−161.
(27) Healy, J.; de Groot, J.; Kestin, J. The theory of the transient hot-wire method for measuring thermal conductivity. *Physica B+C* **1976**, *82*, 392−408.
(28) Kestin, J.; Wakeham, W. A contribution to the theory of the transient hot-wire technique for thermal conductivity measurements. *Phys. A* **1978**, *92*, 102−116.
(29) Das, S. K.; Choi, S. U. S.; Patel, H. E. Heat transfer in nanofluids−A review. *Heat Transfer Eng.* **2006**, *27*, 3−19.
(30) Pastoriza-Gallego, M. J.; Lugo, L.; Cabaleiro, D.; Legido, J. L.; Piñeiro, M. M. Thermophysical profile of ethylene glycol-based ZnO nanofluids. *J. Chem. Thermodyn.* **2014**, *73*, 23−30.
(31) Mariano, A.; Pastoriza-Gallego, M. J.; Lugo, L.; Mussari, L.; Piñeiro, M. M. Co3O4 ethylene glycol-based nanofluids: Thermal conductivity, viscosity and high pressure density. *Int. J. Heat Mass Transfer* **2015**, *85*, 54−60.
(32) Selvam, C.; Lal, D.; Harish, S. Thermal conductivity enhancement of ethylene glycol and water with graphene nanoplatelets. *Thermochim. Acta* **2016**, *642*, 32−38.
(33) Ahammed, N.; Asirvatham, L. G.; Titus, J.; Bose, J. R.; Wongwises, S. Measurement of thermal conductivity of graphene-water nanofluid at below and above ambient temperatures. *Int. Commun. Heat Mass Transfer* **2016**, *70*, 66−74.
(34) Hajjar, Z.; Rashidi, A. M.; Ghozatloo, A. Enhanced thermal conductivities of graphene oxide nanofluids. *Int. Commun. Heat Mass Transfer* **2014**, *57*, 128−131.
(35) Papanastasiou, T. C. Flows of materials with yield. *J. Rheol.* **1987**, *31*, 385−404.
(36) Bingham, E. C. *Fluidity and Plasticity*; McGraw-Hill Book Company, Incorporated, 1922; Vol. 2.
(37) Herschel, W.; Bulkley, R. Konsistenzmessungen von Gummi - Benzollosungen. *Kolloid-Z.* **1926**, *39*, 291−300.
(38) Shih, W.; Shih, W.-H.; Aksay, I. Elastic and yield behavior of strongly flocculated colloids. *J. Am. Ceram. Soc.* **1999**, *82*, 616−624.
(39) Marcovich, N.; Auad, M.; Bellesi, N.; Nutt, S.; Aranguren, M. Cellulose micro/nanocrystals reinforced polyurethane. *J. Mater. Res.* **2006**, *21*, 870−881.
(40) Assael, M.; Antoniadis, K.; Wakeham, W. Historical evolution of the transient hot-wire technique. *Int. J. Thermophys.* **2010**, *31*, 1051−1072.
(41) Cabaleiro, D.; Pastoriza-Gallego, M. J.; Piñeiro, M. M.; Legido, J. L.; Lugo, L. Thermophysical properties of (diphenyl ether + biphenyl) mixtures for their use as heat transfer fluids. *J. Chem. Thermodyn.* **2012**, *50*, 80−88.
(42) Pastoriza-Gallego, M. J.; Lugo, L.; Legido, J. L.; Piñeiro, M. M. Enhancement of thermal conductivity and volumetric behavior of FexOy nanofluids. *J. Appl. Phys.* **2011**, *110*, No. 014309.
(43) Antoniadis, K. D.; Tertsinidou, G.; Assael, M.; Wakeham, W. Necessary Conditions for Accurate, Transient Hot-Wire Measurements of the Apparent Thermal Conductivity of Nanofluids are Seldom Satisfied. *Int. J. Thermophys.* **2016**, *37*, 1−22.
(44) NIST Chemistry Webbook, 2017. http://webbook.nist.gov/chemistry/.
(45) Pastoriza-Gallego, M. J.; Lugo, L.; Legido, J. L.; Piñeiro, M. M. Rheological non-Newtonian behaviour of ethylene glycol-based Fe2O3 nanofluids. *Nanoscale Res. Lett.* **2011**, *6*, No. 560.
(46) Pastoriza-Gallego, M. J.; Pérez-Rodríguez, M.; Gracia-Fernández, C.; Piñeiro, M. M. Study of viscoelastic properties of magnetic nanofluids: an insight into their internal structure. *Soft Matter* **2013**, 11690−11698.

DOI: 10.1021/acsomega.7b01681
ACS Omega 2018, 3, 744−752